DOI: 10.13009/EUCASS2023-693
Aerospace Europe Conference 2023 – 10TH EUCASS – 9TH CEAS

Analysis of Detailed-Chemistry Schemes for the Numerical Simulation of Supercritical LOx/CH_4 Flames

Tim Horchler, Stefan Fechter and Sebastian Karl*
German Aerospace Center (DLR), Institute of Aerodynamics and Flow Technology, Spacecraft Department
Bunsenstrasse 10, 37077 Göttingen, Germany
tim.horchler@dlr.de · stefan.fechter@dlr.de · sebastian.karl@dlr.de
*Corresponding author

Abstract

The increasing interest in reusable LOx/CH_4 first-stage liquid rocket engines requires the further development of suitable computational fluid dynamics tools for the reliable design and analysis of such engines. Shifting from classical LOx/H_2 to methane as a fuel involves many challenges for the accurate modeling of chemical effects as the characteristic time scale for LOx/CH_4 is significantly longer than for hydrogen. This may result in, for example, flame lift-off and reattachment effects that may cause substantial combustion instabilities. Also, the injector wall temperature may play a more significant role than in classical LOx/H2 engines. The purpose of this study is to compare numerical simulation results using a complex detailed-chemistry scheme with previous results obtained with a real-gas flamelet combustion model. Additionally, a novel machine-learning based approach for the efficient tabulation of chemical reactions rates will be tested and compared against results with the full reaction mechanism. This comparison will be based on two dedicated numerical test cases which have been used extensively in the past: The first one is a modified version of the 2D mixing test case proposed in Ruiz et al.[17] This computationally cheap setup allows for a detailed study of mixing and chemical reactions under thermodynamic conditions that are representative for rocket engine. A more realistic setup will be investigated with the second test case HF-10 from the Franco-German Rocket Engine Stability Initiative (REST). In this test case, the flame behind a realistic single shear- coaxial injector will investigated in a 3D simulation at supercritical conditions. This paper continues our work on the HF-10 test case[4,19] presented at the EUCASS 2022 conference and allows for a more general assessment of chemical non-equilibrium effects at supercritical pressures commonly encountered in liquid rocket engines.

1. Introduction

Even though the fuel combination liquid oxygen and hydrogen (LOx/H_2) offers the highest specific impulse of all utilizable fuel combinations, the difficulty in handling (cryogenic) hydrogen is considered a major drawback when it comes new, re-usable and cost-efficient space launcher designs. In recent years, methane (CH_4) has emerged as the most promising substitute fuel for H_2 and is now used in multiple new engine designs around the world, e.g. in the SpaceX Raptor engine, the European Prometheus engine or Blue Origins BE-4 engine. Compared to hydrogen, methane offers a few favorable properties that make it an appealing alternative rocket fuel. Methane has a higher density than hydrogen in its liquid phase, therefore requiring smaller fuel tanks which increases the payload capacity. Due to its higher boiling temperature, it is easier to store and requires less insulation before launch and in space when used in upper stage engines. Methane also has a lower specific heat capacity in the liquid phase which requires less heat for evaporation, therefore increasing the engine efficiency. Additionally, the fuel/oxidizer combination of CH_4/LOx offers the highest specific impulse[18] with regard to other commonly used fuel combinations, like LOx-kerosene or N_2O_4-MMH.

The increasing interest to develop new LOx/CH_4 liquid rocket engines is accompanied by the need for suitable computational fluid dynamics simulations tools. Apart from other modeling aspects like thermodynamic (real gas) models, turbulence models and numerical aspects, the quality of CFD results strongly depends on the suitability of the underlying chemical reaction modeling approach. Modeling chemical reactions in computational fluid dynamics is a challenging task: Apart from numerical problems, stemming from chemical reaction time scales usually being much smaller than turbulent time scales, considerable effort is currently spent in the scientific community in developing reaction mechanism for methane/oxygen combustion.[18,27] Because of its importance to the gas turbine community,

DOI: 10.13009/EUCASS2023-693

many of the published methane combustion mechanism are designed for pressures lower than those typically used in rocket engines. A notable exception is, for example, the Zhukov-Kong mechanism[28] mechanism which has been used in a variety of studies related to this work.[4,10]

Apart from the underlying reaction mechanisms, various models at different levels complexity have been developed in the past years for modeling chemical reactions in CFD solvers. The highest level of modeling complexity is reached with detailed chemistry schemes that explicitly solve transport equations for all participating species and provide their chemical source terms . By further taking into account the interaction between turbulent scales and the flame, (transport-)PDF-models[11] offer a superb modeling fidelity, however, at an often prohibitively high numerical cost. Many approaches have been developed to reduce this very high computational cost. For non-premixed diffusion flames, the flamelet approach[15] allows to reduce the computational effort significantly by pre-tabulating the flame structure and only solving a reduced set of transport equations in the flow solver. This approach has been used in previous studies[1] of liquid-rocket engines at sub- and supercritical conditions. To reduce the computational cost due to the chemistry scheme even further, especially for scale-resolving turbulence modeling methods like Large-(LES) and Detached-Eddy simulations, the eddy dissipation model (EDM) and eddy dissipation concept (EDC) are proposed in the literature. With the increasing interest in LOx/CH_4 for liquid rocket engines also the scientific community changed their focus towards this fuel/oxidizer combination. Recent experimental investigation[13] showed, however, that the flame characteristics and the flame anchoring behavior of LOx/CH_4 can be fundamentally different from the well understood H_2/O_2 reaction system. Modeling flame characteristics and flame-anchoring now requires a much higher level of modeling fidelity. Unfortunately, simplified models like the standard flamelet approach cannot be used to model ignition delay phenomena. The purpose of this paper is therefore to investigate if a detailed chemical reaction scheme can be used to model flame detachment under engine-relevant flow conditions in a simplified test case. Second, a new approach for the reduction of chemical reaction schemes by using tabulated non-Arrhenius reaction rates will be tested.

2. Numerical Setup

This work uses the DLR TAU code,[20] second-order, finite-volume method for solving the compressible Navier-Stokes equations. Upwind fluxes in the cell-centered scheme are calculated using a low-Mach-number[22] corrected version of the MAPS+[16] upwind solver. Time integration towards steady-state is achieved by an explicit Runge-Kutta scheme. In order to speed up the solution process, a local time-stepping approach selects the largest-possible time step size per cell. For the time-accurate unsteady simulations, a Jameson-type[6] dual time stepping approach with a physical time-step size of 5×10^{-7} s for test case HF-10 and 5×10^{-8} s for the modified Ruiz case. All steady RANS simulations use the Wilcox $k-\omega$ turbulence model.[26] For the scale-resolving simulations, a delayed detached-eddy simulation (DDES) scheme,[21] based on a two-equation $k-\omega$ turbulence model,[23] is used. For the real-gas properties of the oxidizer, the Soave-Redlich-Kwong equation-of-state[8] is used. In this paper, three different approaches to combustion modeling are used: The simplest model is an adiabatic flamelet model[15] extended for real-gas effects.[9] In this model, a set of flamelet solutions at different scalar dissipation rates χ is created and then converted into a three-dimensional lookup table. This table is then used in the TAU code to look up the flame composition as a function of mixture fraction Z, the variance of mixture fraction Z''^2 and scalar dissipation rate χ. As only two additional equations need to be solved inside the code irrespective of the number of species used, this model is computationally efficient compared to more detailed approaches of combustion modeling.

2.1 Calculation of the Chemical Source Term

For the calculation of the chemical source terms, we will use the law of mass action together with an classical Arrhenius term for pressure independent reactions. For pressure dependent reactions, the forward reaction rate will be modified according to the approach Lindemann[24] which represents a bridging-function between the high- and low-pressure regime. Assuming a generic reaction r with a forward rate k_r^f and backward rate k_r^b, including an inert species M. The stoichiometric coefficients are given by α_r^s and β_r^s.

$$\sum_s \alpha_r^s X^s + M \underset{k_r^b}{\overset{k_r^f}{\rightleftharpoons}} \sum_s \beta_r^s X^s + M$$

Then, the chemical source term for each species ω^s can be written as

$$\omega^s = M^s \sum_r (\beta_r^s - \alpha_r^s) \left[k_r^f \prod_s [X^s]^{\alpha_r^s} [\tilde{M}_r] - k_r^b \prod_s [X^s]^{\beta_r^s} [\tilde{M}_r] \right] \tag{1}$$

DOI: 10.13009/EUCASS2023-693

where $[\tilde{M}_r]$ denotes the effective concentration of the collision partners with the other reactants:

$$[\tilde{M}_r] = \sum_s \epsilon^s \left(\frac{\rho^s}{M^s} \right)$$

These effectivity factors ϵ^s are provided together with the reaction mechanism. In case there are only two-body reactions without inert partners, the effective concentration then equals one:

$$[\tilde{M}_r] = 1$$

The forward reaction rate is calculated using the Arrhenius function

$$k_r^f = A_r T^{n_r} \exp\left(-\frac{E_r}{R_u T} \right) \tag{2}$$

The backward reaction rate is calculated based on the forward rate and the equilibrium constant using

$$k_r^b = \frac{k_r^f}{K_r^{eq.}}.$$

For pressure-dependent reactions, two sets of independent Arrhenius parameters are given for the high- and low-pressure limit. These result in two forward reaction rates for the high-pressure limit k_r^∞ and the low-pressure limit k_r^0. From these two limits, the effective forward rate is calculated using

$$k_r^f = k_r^\infty \left(\frac{P_{\text{red.}}}{1 + P_{\text{red.}}} \right) F(T, P_{\text{red.}}). \tag{3}$$

This term contains the reduced pressure $P_{\text{red.}}$ given by

$$P_{\text{red.}} = \frac{k_r^0 [\tilde{M}]_r}{k_r^\infty}. \tag{4}$$

Additionally, the Lindemann approach also contains so-called fall-off functions which are usually modelled according to Gilbert et al.[3]

2.2 Tabulation of Forward Reaction Rates

The derivation of the chemical source term in the previous section now suggests an approach to tabulate the forward reaction rate as a function of temperature T and the effective concentration of the collision partners $[\tilde{M}]_r$. This tabulation appears useful for two reasons: First of all, we can avoid the costly computation of the exponential function in the Arrhenius term in Eq. 2. Another benefit of tabulation is the fact that it is not limited to Arrhenius-type reaction but can acommodate any (arbitrary) dependence of the reaction rate on temperature and effective concentration of the collision partners.

As the reduced pressure Eq. 4 is a function of $[\tilde{M}]_r$ and the temperature T (through the high- and low pressure Arrhenius rates) only, also the effective forward rate Eq. 3 for the pressure-dependent reaction is only a function of T and $[\tilde{M}]_r$. With this, the law of mass action Eq. 1 can be even further simplified if the effective concentration of collision partners is moved into a combined forward reaction rate $\tilde{k}_r^f$, which can be tabulated:

$$\tilde{k}_r^f = \tilde{k}_r^f \left(T, [\tilde{M}]_r \right) = k_r^f \cdot [\tilde{M}]_r = k_r^\infty [\tilde{M}]_r \left(\frac{P_{\text{red.}}}{1 + P_{\text{red.}}} \right) F(T, P_{\text{red.}}) \tag{5}$$

Then, the equation for the chemical source term of species s reduces to

$$\omega^s = M^s \sum_r (\beta_r^s - \alpha_r^s) \left[\tilde{k}_r^f \prod_s [X^s]^{\alpha_r^s} - \frac{\tilde{k}_r^f}{K_r^{eq.}} \prod_s [X^s]^{\beta_r^s} \right]$$

This tabulation approach can now be used to handle the different cases that can occur with pressure-dependent and independent reactions:

1. The most simple case is a **two-body reaction** that only depends on the temperature. Here, one has to tabulate the forward reaction $\tilde{k}_r^f$ rate solely as a function of temperature T: $\tilde{k}_r^f = k_r^f(T)$

DOI: 10.13009/EUCASS2023-693

2. For a **pressure-independent three-body reaction**, the effective concentration of the collision partners does alter the forward reaction rate and can therefore be calculated as a multiplication factor in the law of mass action. Also, the forward reaction rate is only tabulated as a function of temperature and then multiplied by the effective concentration: $\tilde{k}_r^f = k_r^f(T) \cdot [\tilde{M}]_r$
3. The most complex case is a **pressure-dependent three-body reaction**. As the effective concentration of the collision partners enters the reduced pressure, one has to tabulate the forward reaction rate as a function of both temperature T and $[\tilde{M}]_r$, therefore $\tilde{k}_r^f = k_r^f\left(T, [\tilde{M}]_r\right)$

For the modeling of methane-oxygen combustion at pressures of approximately 100 bar, this work uses the skeletal mechanism of Zhukov and Kong.[28] Containing 22 species and 49 reactions, it is used as the reference mechanism in this work without any tabulation. Also the flamelet combustion model is based on this reaction mechanism.

The Zhukov-Kong mechanism also serves as the basis for a further reduction based on neural networks. This reduction approach is outlined in further detailed in the work of Karl[7] in the same conference. The goal is to considerably reduce the 49 reaction skeletal mechanism of Zhukov and Kong by applying neural network prediction outlined by Karl[7] while still giving correct reactions rates in the vicinity of the 100 bar operating point. For this, two steps are necessary. First, the optimized reaction rates are allowed to be arbitrary functions of temperature and pressure, therefore abandoning a strict Arrhenius-based approach. Second, the new arbitrary reaction rates model an extended version of the Westbrook and Dryer[25] reaction mechanism:

$$\begin{aligned} 2CH_4 + 3O_2 &\rightarrow 2CO + 4H_2O \\ 2CO + O_2 &\rightarrow 2CO_2 \\ H_2O + O_2 &\rightarrow O + 2OH \\ CO + H_2O &\rightarrow CO_2 + 2H \end{aligned}$$

The forward rates $\tilde{k}_r^f$ for these reactions are now tabulated as a function of temperature only, as no pressure dependent reactions are used in the modified Westbrook-Dryer scheme. The equidistant reaction rate table spans a temperature range from 80 K to 6000 K covering the whole chemical state space.

3. Results

This section will present simulation results for two different test cases. The first one is the purely numerical test case published by Ruiz et al.[17] in 2015. Originally intended for the study of supercritical mixing, this test case has been extended in the past years towards reacting simulations.[2,12] This test case is highly attractive for mainly two reasons: Due to its two-dimensional setup, it requires only a limited of amount of computational resources to provide meaningful results. Second, almost all modeling aspects (numerical scheme, discretization approaches, chemical modeling, real-gas thermodynamic modeling) necessary for the simulation of liquid rocket engines can be tested, except a fully three-dimensional scale-resolving turbulence model. However, even though a two-dimensional Large- or Detached-Eddy simulation can never fully account for the inherently three-dimensional nature of turbulent structures, the test case still allows for in-depth testing and verification before the setup is applied to computationally much more expensive 3D cases. Also added, the test case can be used to simulate operating conditions that are representative for small upper stage engines or model combustion chambers.

The second test case under consideration was developed by the Rocket Engine Stability Initiative (REST). It consists of a realistic single shear-coaxial injection element placed inside a long hexagonal combustion chamber without nozzle. This test case has been used extensively in the past (see e.g. Schmitt et al.[19]) for the comparison of numerical codes.

Both test cases investigated in this paper use the same operating point at 100 bar, T_{O_2} = 100 K and T_{CH_4} = 231 K. They also use the same oxidizer-to-fuel ratio of ROF = 3.81. For the test case of Ruiz, however, no complete combustion is reached and only the near-injector field is investigated.

3.1 Test case of Ruiz et al.

Fig.1 shows a schematic setup of the Ruiz test case used in this setup. The lip height h shown in this figure is 0.5 mm and therefore representative of a typical injector lip. For a proper resolution of the shear layer formation, the injector lip is discretized with 100 structured (cubical) cells whose stretching increases towards upper and lower sides of the computational domain. Altogether, the grid consists of approx. 1.07 Mio. grid points.

The simulation of the Ruiz test case is run with dual-time stepping scheme at a physical time step size of 5×10^{-8} s. For the mean quantities, simulation results are ensemble averaged over multiple time steps.

DOI: 10.13009/EUCASS2023-693

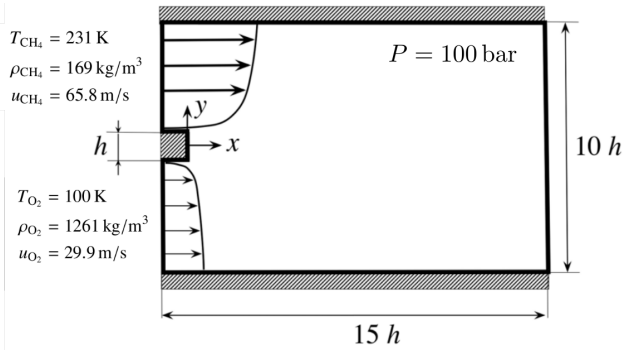

Figure 1: Setup and inflow conditions modified from the Ruiz test case.[17]

3.2 Investigation of Flame Detachment

The first investigation is concerned with flame detachment and flame-anchoring in liquid rocket engines. Due to its slower chemical time scale, the CH_4/O_2 reaction system is much more susceptible to flame detachment than the fast reactions of H_2/O_2. Also recent experimental investigations[13] suggest that intermittent flame anchoring occurs under various operating conditions. Investigating this effect numerically requires a large computational effort as the chemical time scales (and reaction paths) need to be modeled appropriately. Therefore, detailed reaction mechanisms are indispensable.

In order to investigate flame anchoring, the injector lip wall temperature is varied for the Ruiz test case, and the results are presented hereafter.

Figs. 2 show the instantaneous temperature field in die flow field behind the injector lip at adiabatic conditions and for two fixed wall temperatures (500 K and 250 K). While the overall flow field structure remains essentially the same, the near-injector region shows a few differences.

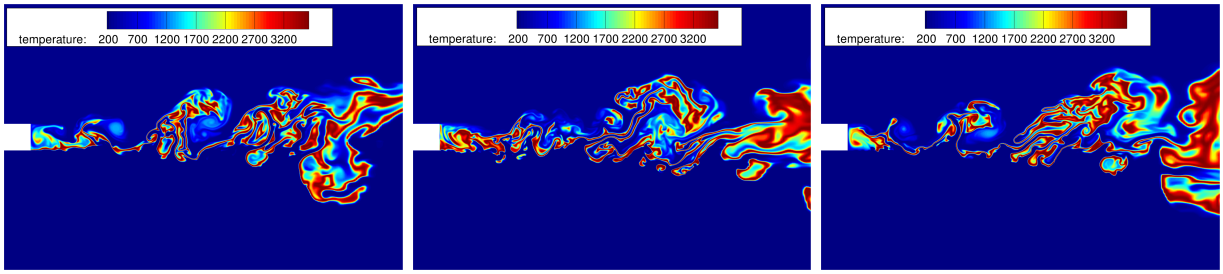

(a) Adiabatic wall (b) T_{Wall} = 500 K (c) T_{Wall} = 250 K

Figure 2: Instantanious snapshots of the temperature field for Ruiz test case.

The near-wall region is dominated by the recirculation of hot gas leading to a stable flame anchoring in the case of an adiabatic wall. A shear layer of hot, reacting gas forms at the lower (O_2) side of the lip and stays attached to the wall. While the same holds for the wall at 500 K, this shear layer completely vanishes for a wall temperature of 250 K. Even though in all cases a strong recirculation zone is formed, only the adiabatic wall case and the wall temperature of 500 K contains this reacting shear layer.

This shear layer is also well visible in the OH partial density ρ_{OH} image, shown in Figs. 3. As a marker of the chemical reaction zone, this variable is a better indicator for the location of the flame, and therefore, flame anchoring.

For the wall temperature of 250 K, one notices flame lift-off from the lip which is not visible in the snapshots at other wall temperatures. For the given instant of time, the flame-detachment could be observed for the wall temperature of 250 K while at other times (not shown), the flame seemed to be anchored at the wall again. In order to investigate the average state of flame anchoring, Figs. 4 shows the time-averaged field value of the OH mass fraction $Y_{OH} = \rho_{OH}/\rho$.

In this picture, one clearly recognizes the attached flame for the adiabatic wall case, indicated by the high mean value of OH mass fraction near the lower edge of the injector lip. Interestingly, the time averaged OH field for the 500 K case shows high mass fractions along the full width of the injector lip and in the recirculation region. This picture then changes for a wall temperature of 250 K: Here, no amount of OH mass fraction is visible directly adjacent the wall and there is only little OH concentration in the recirculation zone.

DOI: 10.13009/EUCASS2023-693

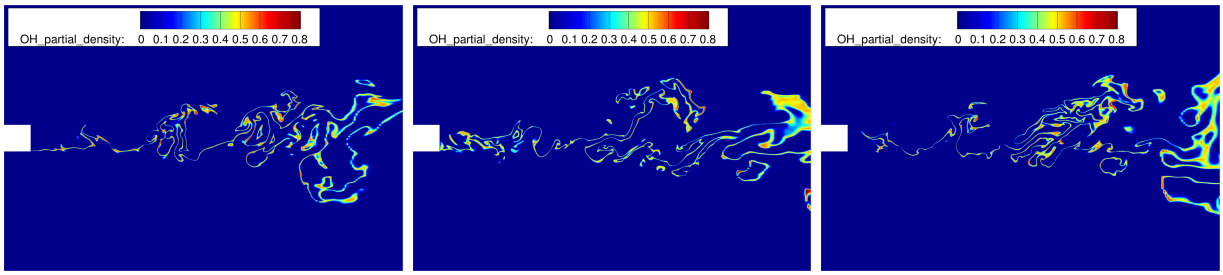

(a) Adiabatic wall (b) T_{Wall} = 500 K (c) T_{Wall} = 250 K

Figure 3: Instantaneous snapshots of the OH partial density field for Ruiz test case.

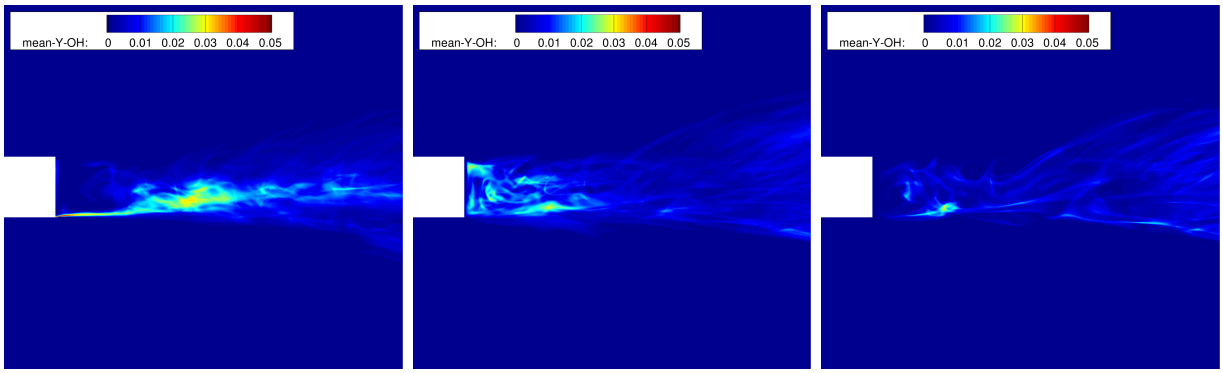

(a) Adiabatic wall (b) T_{Wall} = 500 K (c) T_{Wall} = 250 K

Figure 4: Time-averaged OH mass fraction field for Ruiz test case.

To the best of the author's knowledge, there are currently no experimental measurements of the lip wall temperature available. Therefore, one cannot give a clear indication if the assumption of 500 K or even 250 K is realistic. Due to it's small size and thickness compared to the overall chamber size, one would also need a proper solid material heat conduction model to assess the lip temperature appropriately. However, the wall temperature range investigated is likely closer to the true value than the adiabatic wall temperature of 2000 K - 2100 K which has been extracted from the time-averaged experimental data. Therefore, it appears reasonable that flame detachment will occur at conditions relevant to liquid rocket engines.

3.2.1 Evaluation of the Reduced Chemistry Scheme

The previous investigation showed that flame anchoring is strongly influenced by the lip's wall temperature and that flame detachment might occur at engine-relevant conditions. While these results could be obtained with the full 22 species 49 reaction Zhukov-Kong mechanism[28] for the 2D Ruiz test case, it is computationally very demanding to use such a complex mechanism for full 3D configurations. Therefore, simpler combustion models need to be investigated that could still account for flame detachment. One possibility might be the flamelet-progress-variable model of Ihme et al.[5] It is, however, still bound to the typical flamelet assumption of a constant Lewis number Le = 1. Additionally, an extension to non-adiabatic walls is possible, but requires some effort.[14] Therefore, simplified detailed chemistry schemes could be an efficient option to still account for flame-anchoring effects while being computationally attractive.

In this section, we will compare simulation results from the standard flamelet model, the detailed chemistry scheme with 22 species and the reduced scheme that is described in the method section above.

Fig. 5 shows a comparison of the instantaneous temperature field behind the injector lip. Comparing the field from the flamelet simulation (left) to the full detailed chemistry simulation (middle) shows a larger opening angle for the detailed chemistry scheme. As expected, both flames are fully attached to the lip and the overall length of the individual coherent eddies, about the size of the injector lip, appears to be similar. The situation is different for the reduced chemistry scheme simulation (shown in the right picture) which exhibits much larger region of intermediate temperatures (approximately 1500 K) which surround the reaction region towards the fuel rich side. Also, the opening angle of the shear layer is similar to the flamelet solution but unlike the full detailed chemistry scheme.

A similar situation is observed for the density mixing, shown in Fig. 6.

DOI: 10.13009/EUCASS2023-693

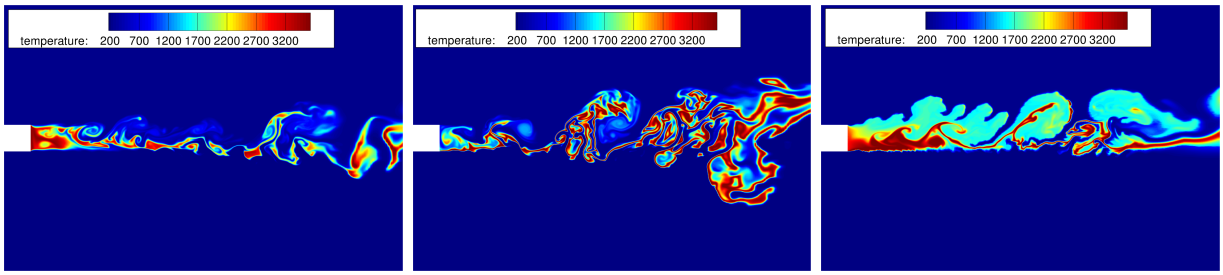

(a) Flamelet model (b) Full detailed chemistry scheme (c) Reduced detailed chemistry scheme

Figure 5: Instantaneous snapshot of the temperature field.

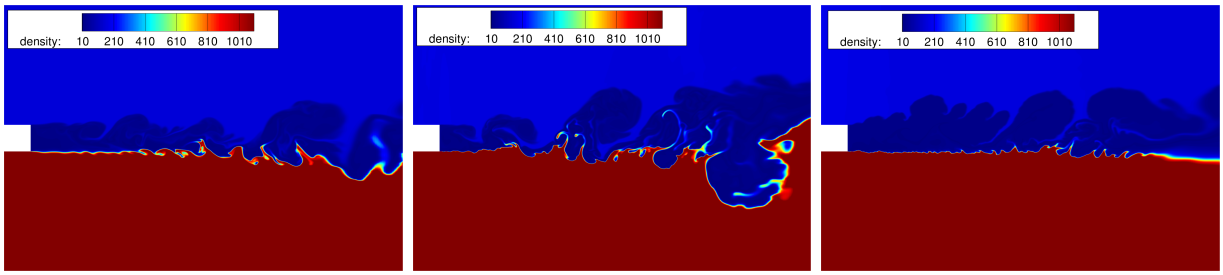

(a) Flamelet model (b) Full detailed chemistry scheme (c) Reduced detailed chemistry scheme

Figure 6: Instantaneous snapshot of the density field.

The reduced chemistry scheme shows even smaller turbulent eddies at the CH_4-O_2 interface than the flamelet simulation. Here again, the full detailed chemistry scheme shows rather large eddies downstream of the injector lip.

In order ensure that these observations are not only instantaneous feature of one solution but persist even in the time-averaged results, Fig. 7 compares time-averaged results of the temperature field.

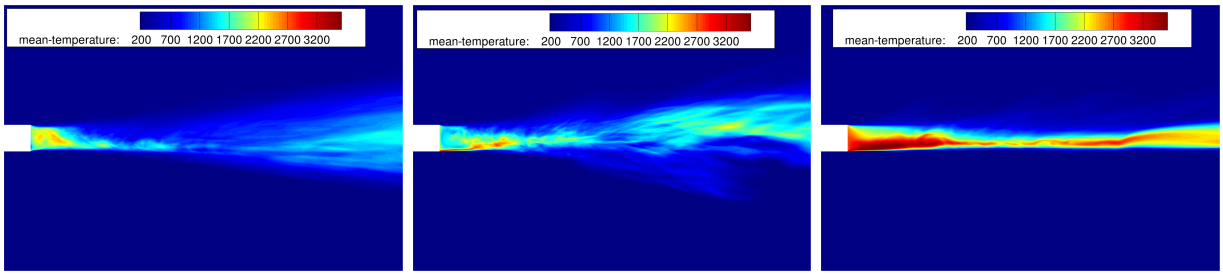

(a) Flamelet model (b) Full detailed chemistry scheme (c) Reduced detailed chemistry scheme

Figure 7: Time-averaged temperature field.

Here, the differences between the three combustion models become even more apparent. The flamelet and the fully detailed chemistry simulation are qualitatively similar, i.e. high temperature near the lip, then an expansion zone with lower temperature, resulting in again rising temperature further downstream. For the reduced chemistry scheme, the temperature field is much more in lateral direction while the time-averaged reaction zone is much thicker than for the other two simulations.

The reason for this behavior is not readily apparent from the flow field plots shown above. Therefore, the flame structure is investigated with two scatter plots in Fig. 8

The scatter plot of the flame temperature shows the flame structure as a function of the mixture fraction Z. By comparing the flamelet (orange) and the full detailed chemistry solution (blue), we can recognize the typical structure of a diffusion flame. The maximum temperature is reached for the stoichiometric value (around $Z = 0.2$) and a subsequent drop to the inflow temperatures on the oxidizer side ($Z = 0$) and fuel side ($Z = 1$). One apparent difference between the flamelet (orange) and the full detailed chemistry solution are states between the equilibrium and the mixing curve, i.e. temperatures lower than the equilibrium temperature at intermediate mixture fractions $0 < Z < 1$. While the flamelet model accounts for turbulence-flame interaction by the built-in presumed β-pdf model, all detailed chemistry

DOI: 10.13009/EUCASS2023-693

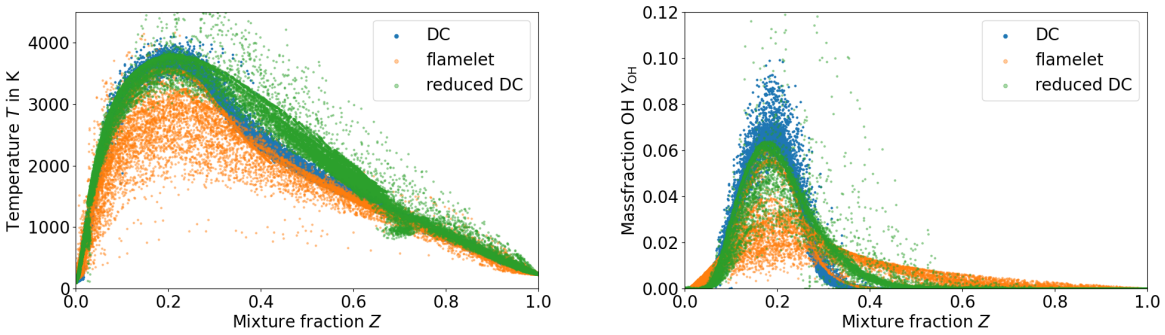

Figure 8: Scatter plots showing the flame structure in mixture fraction Z-space. The left plot shows the temperature structure of the flame while the right plot shows OH mass fraction as a marker of the main reaction zone.

simulations here are laminar in a sense that the reaction rate does not account for turbulence effects on the temperature and mixture composition field. For the flamelet model, this results in generally lower temperatures and a lower heat-release rate. Therefore, one would expect a smaller opening angle of the reacting shear layer as it is observed in the simulations.

The reduced chemistry scheme, however, shows a different situation. A first problem with this can be seen in the region of $Z = 0.4$ where the full detailed reaction mechanism and the flamelet model show a drop in temperature compared to the reduced detailed chemistry scheme. This drop in temperature is typical for hydrocarbon-based fuels and does not appear for a H_2/O_2 reaction schemes. As the reduced the chemistry scheme fails to predict this behavior, the resulting flame shape resembles more like a hydrogen-oxygen scheme. This also explains the largely increased zone of intermediate temperatures seen in Fig. 5: These regions belong to the higher temperature states on the fuel-rich side of the flame at $Z = 0.4$. It can, however, be stated that the reduced chemistry scheme is oversimplified and misses some important aspects of the flame shape. Therefore, further investigations are needed as to why the drop in temperature is missing in the reduced scheme. The most likely explanation is that some important dissociation reactions on the fuel-rich side are missing, and that the reactions for $Z > Z_{stoich}$ are less endothermic than they are in reality. This hypothesis will be checked in a future work.

The second problem is concerned with temperatures higher than the equilibrium temperature of the flame. This is sometimes encountered with convergence problems of the solver when an insufficient number of inner iterations is used in the dual time-stepping approach.

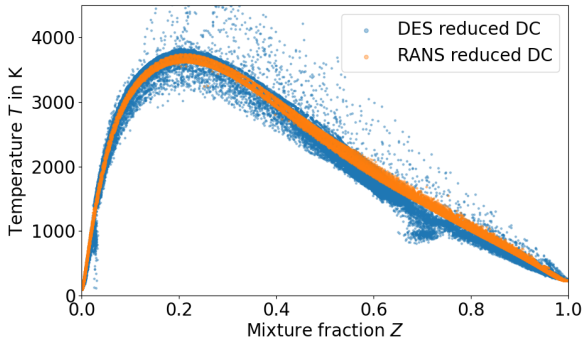

Figure 9: Scatter plot of temperature flame structure for the Ruiz test case. This picture compares results from a steady RANS simulation to the time-averaged DES results.

In order to verify that this indeed a convergence problem, Fig. 9 shows the temperature flame structure for the presumably unconverged detached-eddy simulation (blue) and an fully converged RANS solution (orange). As the RANS simulation does not show any temperatures exceeding the equilibrium curve of the diffusion flame, the conclusion of convergence problems with the reduced detailed chemistry scheme appear reasonable. Here again, the chemistry scheme fails to predict the drop in temperature at $Z = 0.4$ which indicates that the scheme is too reduced and fails to capture important aspects of the flame structure.

In terms of computationally efficiency, it is highly desirable to continue working on the reduced detailed chem-

DOI: 10.13009/EUCASS2023-693

istry scheme and to correct its deficiencies. Profiling the simulations shows that the reduced chemistry scheme, in the way it is currently used, only requires 54 % of the computational resources compared to the full detailed chemistry scheme. This number is likely to increase if more species and reactions need to be added, but it might still compare favorably. In comparison, the flamelet model requires 87 % of the computational cost of the detailed chemistry scheme. However, for a better comparability of the simulation results, the flamelet model has not been optimized and not all possible speed up gains (i.e. tabulating the real-gas cubic mixing coefficients and linearized transport coefficients) have been realized yet. Therefore, a flamelet model can be much more efficient than the one used here.

3.3 Test case HF-10

The HF-10 test case has been proposed by the *Rocket Engine Stability Initiative* (REST) as a common numerical basis for code validation and verification. HF-10 consists of a 300 mm long hexagonal combustion chamber to which a recessed, single shear-coaxial injector is connected. The details of the combustion chamber and the injector dimensions are shown in Fig. 10.

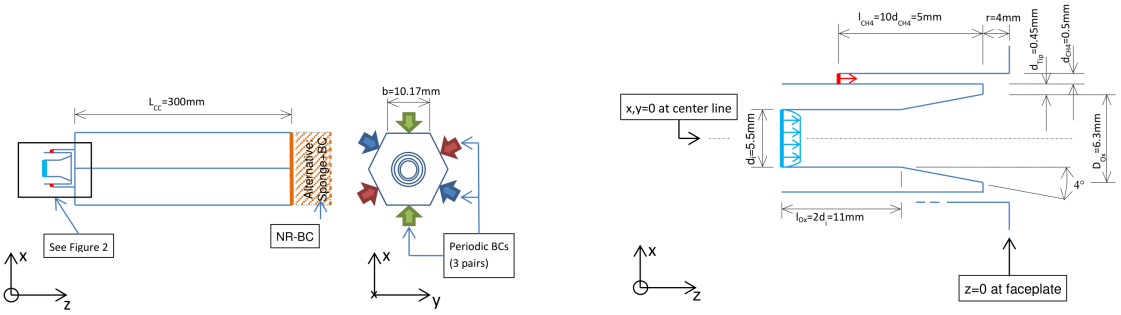

Figure 10: Geometric setup of the testcase. Left: Setup of the whole domain. Right: Size of the coaxial injector.

The results from this test case are presented for the $x = 0$ slice of the computational domain, as shown in Fig. 11.

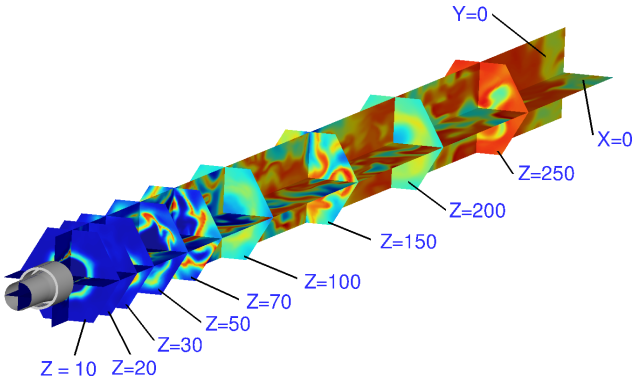

Figure 11: Overview of the different field cuts for HF-10.

Due to numerical stability issues, no converged solution for the reduced detailed chemistry scheme could be obtained. Therefore, only a comparison between two RANS solutions for the steady-state case are presented and the computational requirements for a detailed-chemistry calculation are reported.

Results for the steady-state temperature and density field are shown in the following two plots Fig. 12 and 13. Here, DC refers to the detailed chemistry solution and FL to the flamelet solution.

Even though the detailed chemistry solution (DC) still shows some residual oscillations near the tip of the flame, one clearly notices that the flame length is shorter for the detailed chemistry scheme than for the flamelet model.

This is even more apparent from the density plot in Fig. 13. Unfortunately, no clear explanation for the different flame lengths can be given. When looking at the radially-averaged temperature distribution along the combustion chamber in Fig. 14 (left), there is only a rather small difference between the two simulations. Similarly, the axial velocity does not differ significantly between the two solutions until 220 mm behind the face plate. Downstream of

DOI: 10.13009/EUCASS2023-693

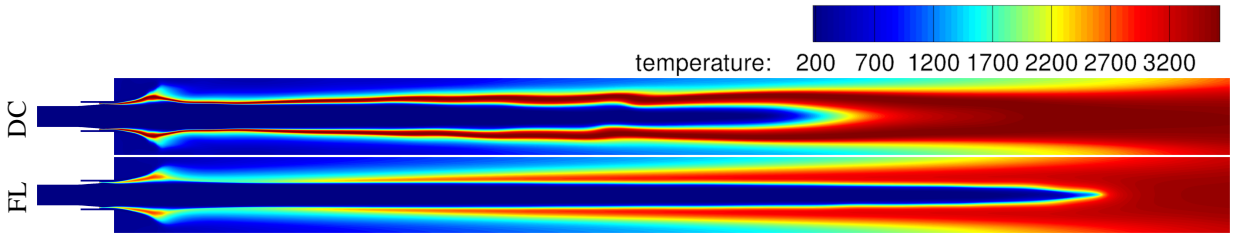

Figure 12: Comparison of the temperature field in the $x = 0$ plane. The contour values are given in K.

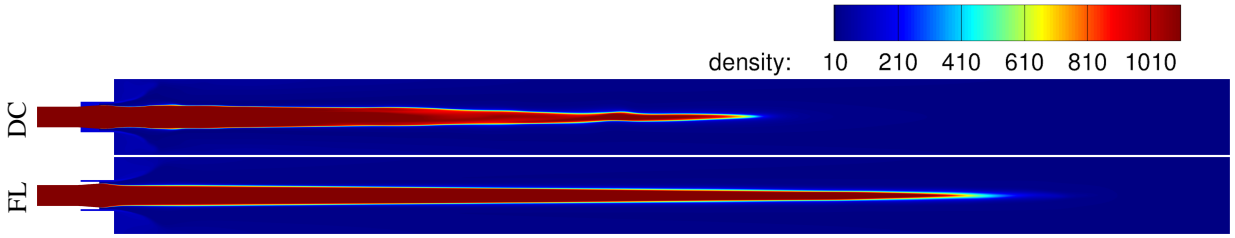

Figure 13: Comparison of the density field in the $x = 0$ plane. The contour values are given in kg/m^3.

this location, the flamelet solutions predicts a much higher axial velocity, caused by a stronger expansion than for the detailed chemistry solution.

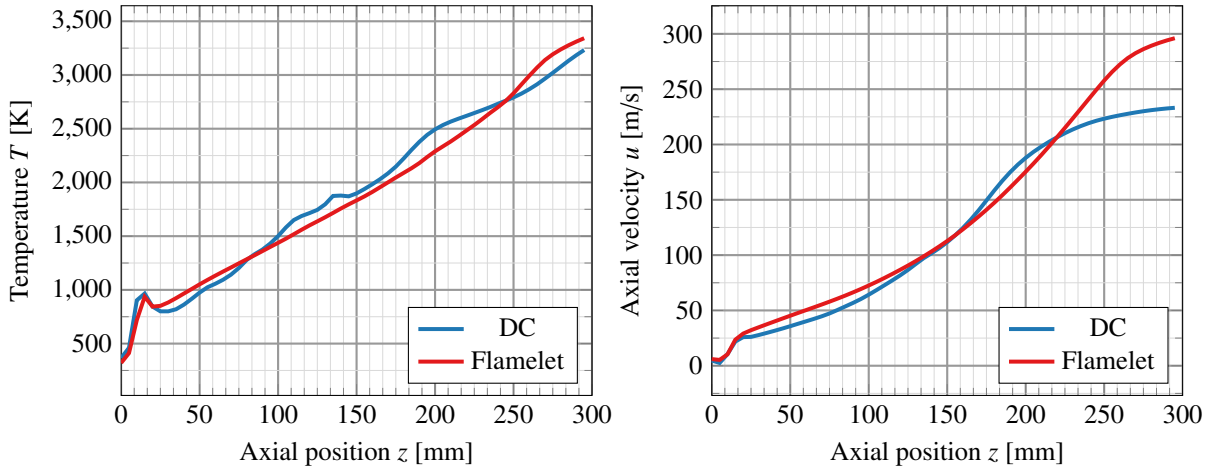

Figure 14: Axial profiles of different flow variables.

Both solutions here predict a similar flow field even though the flame length itself appears to be a very sensitive quantity. In order to improve to predicting capabilities of RANS simulations in this regard, one should consider scale-resolving simulations results (either from DES or related techniques) to validate and improve RANS results. From the computational expense point of view, there is a large difference between the two combustion modeling approaches. The flamelet model only requires approx. 49 % of the computational resources of the detailed chemistry scheme.

4. Summary and Conclusion

This paper presented simulation results obtained with detailed chemical reaction schemes and a flamelet model for two numerical test cases that are representative of realistic liquid rocket engines operated with LOx/CH_4. In the first part of the paper, a tabulation strategy[7] for chemical reaction source terms is presented and later used for a generic non-Arrhenius description of reaction rates. Based on the 22-species reaction mechanism of Zhukov et al.,[28] a study of flame anchoring and flame detachment using the modified version of the numerical test case by Ruiz et al. is presented. Here it is shown that the wall temperature significantly changes the flame attachment behavior leading to detachment

DOI: 10.13009/EUCASS2023-693

when it is set to a low value of 250 K. This result indicates that the injector wall and lip temperature might play a much more important role for LOx/CH_4 combustion than for classical H_2/O_2 engines due to the slower timescales of the chemical reactions. However, this effect can only be investigated by using (computationally expensive) detailed reaction schemes.

In the second part of the result presentation, it is shown that the generic, non-Arrhenius type reaction mechanism based on a 5 species Westbrook-Dryer scheme is too oversimplified to correctly represent the flame. This is best seen in the flame structure scatter plots, where a typical feature of CH_4/O_2 flames is missing. Additionally, the simulation suffered also from convergence problems that resulted in nonphysically high temperatures in some parts of the computational domain. It could be shown by converged RANS solutions of the same test case, however, that the reaction mechanism itself is incomplete and that the convergence issues can be overcome in principle.

The last part of the paper showed detailed-chemistry simulation results for the more realistic HF-10 test case from the Rocket Engine Stability Initiative (REST). Apart from significant differences in the flame length, only small differerences between the flamelet and the full detailed chemistry solution could be found. Both simulation results, however, differ by a factor of two in required computational resources.

This paper showed that flame detachment in liquid rocket engines can be simulated using detailed chemical reaction schemes, however, at a rather high numerical cost. Even though the initial test with a reduced detailed chemical reaction scheme were partially unsuccessful, this approach appears as a promising alternative to other simplified reaction schemes. In the future, it will be tested if the simple Westbrook-Dryer scheme can be extended to account for the effects that are currently missing from the reaction scheme.

5. Acknowledgments

The authors appreciate support from the German Aerospace Center (DLR) project AMADEUS (Advanced Methods for Reusable Aerospace Vehicle Design using Artificial Intelligence and Interdisciplinary Numerical Simulation) focusing on the development of numerical methods for LOx-methane-based engine concepts in future space transportation systems.

References

[1] Paola Breda and Michael Pfitzner. Delayed detached eddy simulations with tabulated chemistry for thermal loads predictions. *Journal of Propulsion and Power*, 37(1):29–46, 2021.

[2] Stefan Fechter, Tim Horchler, Sebastian Karl, and Klaus Hannemann. Generic numerical test case to understand cryogenic methane combustion dynamics. In *Proceedings of the 3rd International Seminar on Non-Ideal Compressible Fluid Dynamics for Propulsion and Power: NICFD 2020*, pages 47–56. Springer, 2021.

[3] RG Gilbert, K. Luther, and J Troe. Theory of thermal unimolecular reactions in the fall-off range. ii. weak collision rate constants. *Berichte der Bunsengesellschaft für physikalische Chemie*, 87(2):169–177, 1983.

[4] Tim Horchler, Stefan Fechter, Jan van Schyndel, and Michael Oschwald. Rest hf-10 test case: Numerical simulation of a single coaxial lox-ch4 injector with forced mass flow oscillations using the dlr tau-code. In *9th European Conference for Aeronautics and Aerospace Sciences (EUCASS)*, pages 1–14, 2022.

[5] Matthias Ihme and Yee Chee See. Prediction of autoignition in a lifted methane/air flame using an unsteady flamelet/progress variable model. *Combustion and Flame*, 157(10):1850–1862, 2010.

[6] Antony Jameson. Time dependent calculations using multigrid, with applications to unsteady flows past airfoils and wings. In *10th Computational Fluid Dynamics Conference*, page 1596, 1991.

[7] Sebastian Karl. Assessment of neural network-based predictions of chemical production rates in cfd solvers. In *Proceedings of the 10th EUCASS nad 9th CEAS Aerospace Conference*, 2023.

[8] Seong-Ku Kim, Hwan-Seok Choi, and Yongmo Kim. Thermodynamic modeling based on a generalized cubic equation of state for kerosene/lox rocket combustion. *Combustion and flame*, 159(3):1351–1365, 2012.

[9] Seong-Ku Kim, Sung-Mo Kang, and Yong-Mo Kim. Flamelet modeling for combustion processes and nox formation in the turbulent nonpremixed co/h2/n2 jet flames. *Combustion science and technology*, 168(1):47–83, 2001.

DOI: 10.13009/EUCASS2023-693

[10] Pasquale Eduardo Lapenna, Giuseppe Indelicato, Rachele Lamioni, and Francesco Creta. Modeling the equations of state using a flamelet approach in lre-like conditions. *Acta Astronautica*, 158:460–469, 2019.

[11] Ansgar Lechtenberg and Peter Gerlinger. Rest hf-10 test case: Flame response to externally excitation of a methane driven rocket combustion chamber. In *9th European Conference for Aeronautics and Aerospace Sciences (EUCASS)*, 2022.

[12] Peter C. Ma, Daniel T. Banuti, Jean-Pierre Hickey, and Matthias Ihme. Numerical framework for transcritical real-fluid reacting flow simulations using the flamelet progress variable approach. In *55th AIAA Aerospace Sciences Meeting*, number 2017-0143, 2017.

[13] Jan Martin, Wolfgang Armbruster, Dmitry Suslov, Robert Stützer, Justin S. Hardi, and Michael Oschwald. Flame characteristics and response of a high-pressure lox/cng rocket combustor with large optical access. *Aerospace*, 9(8), 2022.

[14] Nikolaos Perakis, Christof Roth, and Oskar J Haidn. Development of a non-adiabatic flamelet model for reacting flows with heat loss. In *Space Propulsion Conference*, volume 2018, 2018.

[15] Norbert Peters. *Turbulent combustion*. Cambridge university press, 2000.

[16] Cord-Christian Rossow. Extension of a compressible code toward the incompressible limit. *AIAA journal*, 41(12):2379–2386, 2003.

[17] Anthony M Ruiz, Guilhem Lacaze, Joseph C Oefelein, Raphaeë Mari, Bénédicte Cuenot, Laurent Selle, and Thierry Poinsot. Numerical benchmark for high-reynolds-number supercritical flows with large density gradients. *AIAA Journal*, 54(5):1445–1460, 2015.

[18] Guido Saccone, Paola Breda, Pasquale Natale, and Francesco Battista. Reduced kinetic mechanism for methane/oxygen rocket engine applications: a reliable and numerically efficient methodology. *Combustion Theory and Modelling*, pages 1–27, 2023.

[19] Thomas Schmitt, Roland Kaess, Roland Behr, Stefan Koeglmeier, Oliver Knab, Tim Horchler, Jan Van Schyndel, Justin S Hardi, David Marchal, Sébastien Ducruix, et al. Rest hf-10 test case: Synthesis of the contributions for the simulation of excited methane flames under real gas conditions. In *9th European Conference for Aeronautics and Aerospace Sciences (EUCASS)*, pages 1–15, 2022.

[20] D. Schwamborn, T. Gerhold, and R. Heinrich. The DLR-TAU-Code: Recent applications in reasearch and industry. In *Proceedings of the European Conference on Computational Fluid Dynamics (ECCOMAS)*, 2006.

[21] Philippe R Spalart, Shur Deck, Michael L Shur, Kyle D Squires, M Kh Strelets, and Andrei Travin. A new version of detached-eddy simulation, resistant to ambiguous grid densities. *Theoretical and computational fluid dynamics*, 20(3):181, 2006.

[22] B. Thornber, A. Mosedale, D. Drikakis, D. Youngs, and R.J.R. Williams. An improved reconstruction method for compressible flows with low mach number features. *Journal of Computational Physics*, 227(10):4873 – 4894, 2008.

[23] A Travin, M Shur, MM Strelets, and PR Spalart. Physical and numerical upgrades in the detached-eddy simulation of complex turbulent flows. In *Advances in LES of complex flows*, pages 239–254. Springer, 2002.

[24] Tamás Turányi and Alison S Tomlin. *Analysis of kinetic reaction mechanisms*. Springer, 2014.

[25] Charles K Westbrook and Frederick L Dryer. Simplified reaction mechanisms for the oxidation of hydrocarbon fuels in flames. *Combustion science and technology*, 27(1-2):31–43, 1981.

[26] David C Wilcox. Reassessment of the scale-determining equation for advanced turbulence models. *AIAA journal*, 26(11):1299–1310, 1988.

[27] Niklas Zettervall, Christer Fureby, and Elna J. K. Nilsson. Evaluation of chemical kinetic mechanisms for methane combustion: A review from a cfd perspective. *Fuels*, 2(2):210–240, 2021.

[28] V.P. Zhukov and A.F. Kong. Development of a skeletal kinetic mechanism of methane oxidation for high pressures and temperatures. In *Proceedings of the Space Propulsion Conference, Rome*, 2016.